Fabrication and Spatially Resolved Functionalization of 3D Microstructures via Multiphoton-Induced Diels–Alder Chemistry

Alexander S. Quick, Hannah Rothfuss, Alexander Welle, Benjamin Richter, Joachim Fischer, Martin Wegener, and Christopher Barner-Kowollik**

Three-dimensional microstructures are fabricated utilizing direct laser writing combined with a non-radical step polymerization based on multiphoton-induced Diels–Alder chemistry of *o*-quinodimethanes and maleimides. Woodpile photonic crystals with a total of five axial periods and a rod spacing of down to 500 nm are fabricated. The structures are characterized via scanning electron microscopy and focused ion beam milling. In addition, corresponding photonic stop bands are investigated via light microscopy as well as transmission and reflection spectroscopy. The Diels–Alder based network formation during direct laser writing is verified via infrared spectroscopy. Spatially resolved surface patterning of covalently bonded functional molecules on fabricated structures is demonstrated by employing the direct laser writing setup and a bromine containing maleimide. The successful surface modification is verified via time-of-flight secondary ion mass spectrometry.

1. Introduction

Micro- and nanodevices have recently experienced increasing attention in the scientific community due to their applicability in a large range of scientific fields. Synergetic know-how between these fields has proven to be beneficial for device fabrication and has provided a better understanding and successive optimization of the overall process. Depending on the shape and dimension of the envisaged device, several fabrication techniques have evolved to meet the practical requirements. For the generation of high resolution two-dimensional (2D) structures, electron or focused ion beam lithography[1] can be employed and nanoimprint techniques allow for high throughput device fabrication.[2] Gray-tone electron beam lithography allows for elevated structure topographies, yet arbitrary three-dimensional (3D) objects are not accessible. Layer-by-layer electron beam lithography enables a larger variety of geometries.[3] However, this technique is time consuming, error prone and restricted to layered geometries. In order to overcome these obstacles, alternative methods have been developed that allow the facile and rapid fabrication of almost arbitrary 3D devices. One of the most versatile techniques is direct laser writing (DLW),[4–7] which has been steadily refined over the past decade and has proven to be a powerful tool for the production of a range of different devices, for example, microelectrochemical systems,[8] optical waveguides,[9] photonic crystals,[10,11] biological scaffolds,[12,13] quantum-photonic circuits,[14] and lab-on-a-chip systems.[15]

The core DLW setup typically consists of a photoresist placed on a sample sheet, a pulsed laser that is focused into the photoresist and a stage capable of moving the sample sheet precisely in three dimensions. Nano-position stages and femtosecond pulsed lasers are commonly employed for the fabrication process. In some cases, picosecond[16] or continous-wave lasers[17] can be used as well. The photoresist itself is transparent to the wavelength of the laser. The use of a pulsed laser system is beneficial when aiming at non-linear optical absorption. Such lasers express a low average power while the peak intensity during a pulse and within the focus is high. By tightly focusing the beam into the photoresist, multi-photon

A. S. Quick, H. Rothfuss, Dr. A. Welle, Prof. C. Barner-Kowollik
Preparative Macromolecular Chemistry
Institut für Technische Chemie und Polymerchemie
Karlsruhe Institute of Technology (KIT)
Engesserstraße 18, 76131 Karlsruhe, Germany
E-mail: christopher.barner-kowollik@kit.edu

A. S. Quick, H. Rothfuss, Dr. A. Welle, Prof. C. Barner-Kowollik
Institut für Biologische Grenzflächen
Karlsruhe Institute of Technology (KIT)
Hermann-von-Helmholtz-Platz 1
76344 Eggenstein-Leopoldshafen, Germany

B. Richter
Zoologisches Institut and Center for Functional Nanostructures
Karlsruhe Institute of Technology (KIT)
Haid-und-Neu-Str. 9 (MRI), 76131 Karlsruhe, Germany

Dr. J. Fischer, Prof. M. Wegener
Institut für Nanotechnologie
Karlsruhe Institute of Technology (KIT)
Hermann-von-Helmholtz-Platz 1
76344 Eggenstein-Leopoldshafen, Germany
E-mail: martin.wegener@kit.edu

Prof. M. Wegener
Institut für Angwandte Physik and Center
for Functional Nanostructures (CFN)
Karlsruhe Institute of Technology (KIT)
Wolfgang-Gaede-Straße 1, 76131 Karlsruhe, Germany

DOI: 10.1002/adfm.201304030

absorption occurs efficiently. As the two-photon absorption rate is proportional to the squared intensity, the absorption is confined to a small volume around the geometrical focus with the highest density of excited molecules being in its center. Excited molecules subsequently undergo chemical reactions, resulting in a solubility change throughout the exposed volume. By moving the laser focus and the substrate relative to each other, the targeted 3D architecture is written into the resist. During the subsequent development step, the soluble constituents of the sample are removed, yielding the targeted structure.

Photoresists consist of different chemical compounds, some of which are sensitive to light. Generally, the curing of these resists can be divided into two types. In positive-tone photoresists, structures are fabricated via focusing the laser beam into a solid resist, thereby solubilizing the exposed volume, while in negative-tone photoresists the exposed volume is permanently solidified (and hence rendered insoluble) in the focus. To date, several negative photoresist systems have been employed for DLW. Most commonly, free radical chain polymerization (CP) occurs during the solidification step. The corresponding liquid resist systems usually consist of a photoinitiator and multifunctional monomers. In the exposed volume the initiating molecules are excited via two-photon absorption and generate radicals that initiate polymerization. Since multifunctional monomers are employed, the polymerization process leads to the generation of crosslinked, insoluble polymeric material in the exposed volume. Common monomers for these photoresists are acrylates with 3–5 functional groups per monomer molecule and polymerization is typically conducted in bulk. Blends of acrylate monomers are also often utilized.[18] A variety of different photoinitiators have been employed for DLW, ranging from cyclic benzylidene ketone-based initiators with high two-photon absorption cross sections[19,20] to commercially available photoinitiators originally developed for UV curing such as Irgacure 369 and Darocur TPO or fluorescent ketocoumarin derivatives utilized for diffraction-unlimited DLW.[21] A similar system, also employing free radical CP during the photofixation step, utilizes organic-inorganic hybrid materials.[22–24] These photoresists make use of the so-called sol-gel process, where an inorganic network (gel) is formed prior to exposure. In this way, volume losses during photopolymerization can be reduced. Besides radical processes, cationic CP of epoxide-containing resists can be employed for DLW such as the widely used SU-8.[11] Herein, the polymerization is photoinitiated via a triarylsulfonium salt, crosslinking the multifunctional epoxide containing molecules (Epon SU8) to form an insoluble network material. All of the here mentioned resists have in common that the chemical reaction during the fixation step follows a CP mechanism. Recently, radical thiol-ene polymerization was introduced to DLW, thereby adopting a radical step polymerization mechanism to microscopic 3D lithography.[25,26]

In the current study, we introduce a photo-triggered click reaction[27] as modular building block in DLW, combining the benefits of photoclick chemistry with the fabrication of functional 3D structures. The polymerization proceeds via a non-radical step mechanism where insoluble crosslinked material is generated via a photo-triggered Diels–Alder reaction (see **Figure 1**a and Section 3). The resist consists of a multifunctional maleimide containing polymer, a tetrafunctional *o*-quinodimethane precursor molecule and a mixture of solvents. Employing this resist, woodpile photonic crystals with a rod spacing ranging from 700 nm to 500 nm were fabricated as test structures and characterized via scanning electron microscopy (SEM) and focused ion beam milling (see Section 4). The optical properties of the photonic crystals were further characterized via transmittance and reflectance spectroscopy as well as light microscopy. In addition, the polymerization mechanism was verified via Fourier transform infrared spectroscopy, where the disappearance of aldehyde related absorption peaks (corresponding to the starting material) was observed as well as the appearance of an alcohol absorption peak (corresponding to the Diels–Alder cycloproduct) for DLW written structures (see Section 5). Further, residual *o*-quinodimethane precursor groups on the surface of fabricated structures could be directly addressed via a subsequent photo-induced Diels–Alder reaction with a functional maleimide (see Figure 1b and Section 6). By employing the DLW setup, spatially resolved surface patterning of covalently bonded functional moieties on fabricated structures was performed. By utilizing a bromine functionalized maleimide, the presence of the halogen atom stemming from the surface patterning procedure was verified by time of flight secondary ion mass spectrometry (ToF SIMS) measurements.

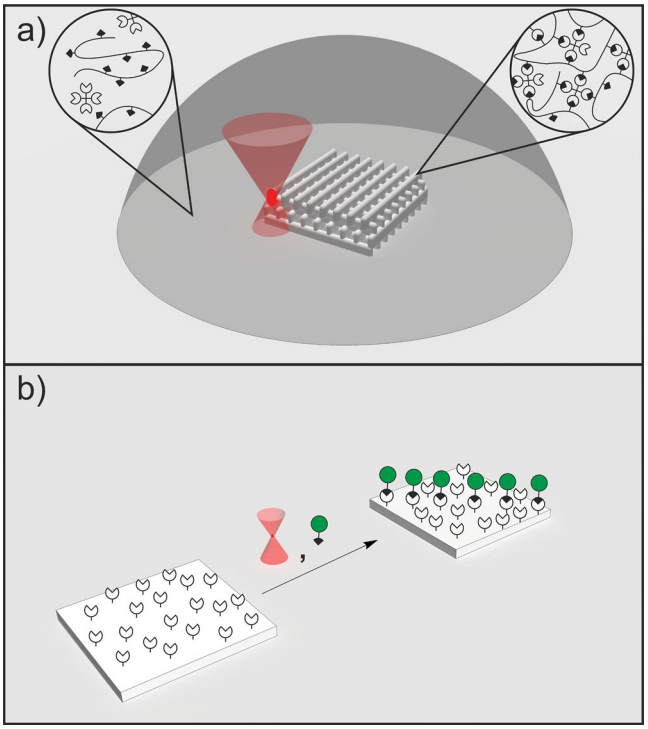

Figure 1. a) Schematic description of a structure being fabricated via photoenol-mediated DLW. The uncured photoresist consists of two active components each bearing one type of functional group. After curing, the functional groups have reacted, forming an insoluble covalently bonded network. b) Spatially resolved patterning employing residual *o*-quinodimethane precursor groups and functional maleimides can be performed on the surface of fabricated structures in the DLW setup. Covalent functionalization occurs only in the exposed areas.

2. General Considerations

A polymerization system suitable for a negative-tone resist in DLW must fulfill certain criteria. Active species generation must be light-induced and polymerization should lead to the rapid formation of insoluble, stable material throughout the exposed volume. For the fabrication of high resolution structures the diffraction limit sets a lower limit from the optics side.[28] Moreover, shrinkage during polymerization and shrinkage during development limit the achievable resolution. Classical non-radical step polymerizations such as polycondensation or polyaddition have been deemed unsuitable for DLW to date as they are thermally initiated and require a high degree of conversion (compared to CP processes) for the formation of insoluble network material. However, non-radical step polymerization techniques offer key advantages in comparison to CP and radical thiol-ene based techniques. During common CPs and radical thiol-ene polymerization utilized in DLW, only the generation of initiating fragments is light triggered. The following polymerization events, however, are independent of irradiation. In a liquid negative-tone resist, the associated active species can diffuse freely. Every propagation event sustains the active species. Propagating species can therefore leave the exposed volume and still continue to polymerize, thereby solidifying unexposed areas and lowering the achievable resolution. For non-radical step polymerizations such as the system presented in the present study the situation is fundamentally different. While the generation of the active species is light induced, active species are consumed, not sustained in the crosslinking reaction. Each active species only induces one polymerization step. Therefore, in sharp contrast to CP and radical thiol-ene polymerization, these fragments may still diffuse out of the exposed volume, yet they do not continue to polymerize since every single linkage reaction must be individually light-activated in the here presented technique. The soluble oligomers therefore either remain idle in the non-exposed volume of the resist or reenter the currently active reaction volume where they then can be readily incorporated into the ongoing network formation.

One important aspect for the good applicability of free radical polymerization in DLW is the high reactivity of free radicals in comparison with other functional groups, making them efficient polymerization species. However, radicals can also undergo various side reactions with a large range of organic functional groups that may be added to the resist in order to optimize optical or mechanical properties of the fabricated structure. These side reactions may alter the fabrication process parameters and structural properties in an unforeseen way or even lead to the failure of the entire fabrication process. The same holds true for cationic polymerization in DLW where epoxides are employed as monomers. These molecules are also highly reactive due to the high ring strain of the functional group which makes them sensitive to reactions with, for example, nucleophiles. Naturally, a high reactivity is mandatory for a successful DLW process and always comes at the price of potential side reactions with other components of the photoresist. However, components that are problematic for radical or cationic reactions are not necessarily problematic for Diels–Alder based photo-polymerizations and could be added into such a resist without altering the polymerization process during fabrication. Thus, it is highly important to increase the toolbox of available polymerization chemistries for DLW by this entirely different mechanism.

3. Polymerization Reagents and Process

In order for step polymerization to function in DLW, a reaction must be employed that is highly efficient, rapid and results in stable covalent bonding of the monomer units. The above mentioned Diels–Alder click reaction fulfills these criteria.[29] Moreover, either the reaction itself or the generation of the reactive species must be light triggered. According to the Woodward-Hoffmann rules, [4+2] Diels–Alder cycloadditions are thermally induced. Therefore, only the generation of the reactive species can be light-induced. This can be accomplished by photoenolization which has been known to the scientific community for about half a century.[30] Early studies on benzophenone derivatives showed that *o*-alkyl substituents bearing hydrogen atoms in α position lead to a suppression of the expected photoreduction to benzopinacol. Instead, an intramolecular rearrangement including hydrogen abstraction leads to the formation of a ground-state photoenol species. This *o*-quinodimethane species can also be generated from corresponding aldehydes and functions as an active diene for the conventional Diels–Alder reaction with dienophiles.[31] The combination of the photoinduced generation of the active diene species and the subsequent reaction with reactive dienophiles has recently proven to be an efficient protocol for the synthesis of complex polymer functionalization and an efficient reaction for the formation of block copolymers.[32,33] Polymeric films have also been generated via this technique in a step polymerization approach.[34] In the current work, we introduce a novel molecule with four active moieties that can undergo efficient photoenolization. The tetralinker **1** can be synthesized from 2,3-dimethylanisole in a four step procedure (see **Figure 2**a and Figure S1, Supporting Information). For the dienophile counterpart, the copolymer compound **2** consisting of methyl methacrylate and a maleimide containing methacrylate was generated via atom transfer radical polymerization. After deprotection of the maleimide, the polymer exhibited a molecular weight of 10 500 g mol^{-1}, a dispersity of 1.2 and close to 12 maleimide groups per polymer chain (see Figure 2b and Figure S2, Supporting Information). The corresponding protected maleimide functional monomer can be synthesized from maleic anhydride in three steps.[35] A polymer component was chosen for DLW as it allows for a high number of functional groups per molecule, lowering the overall conversion that is necessary for solid material generation. Together, these two components are dissolved in a solvent mixture to form the final photoresist. As during the photoenolization process an intramolecular hydrogen transfer takes place, it is important to note that the usage of aprotic solvents is crucial for efficient *o*-quinodimethane formation. During the formation of the *o*-quinodimethane the aromatic system of the photoactive group is lost. After the Diels–Alder reaction with a dienophile, the aromatic system is restored (see Figure 2c). This rearomatization evokes two important features. Firstly, the formation of an aromatic system additionally enhances the already large driving force of the reaction. Secondly, unintended retro-Diels–Alder

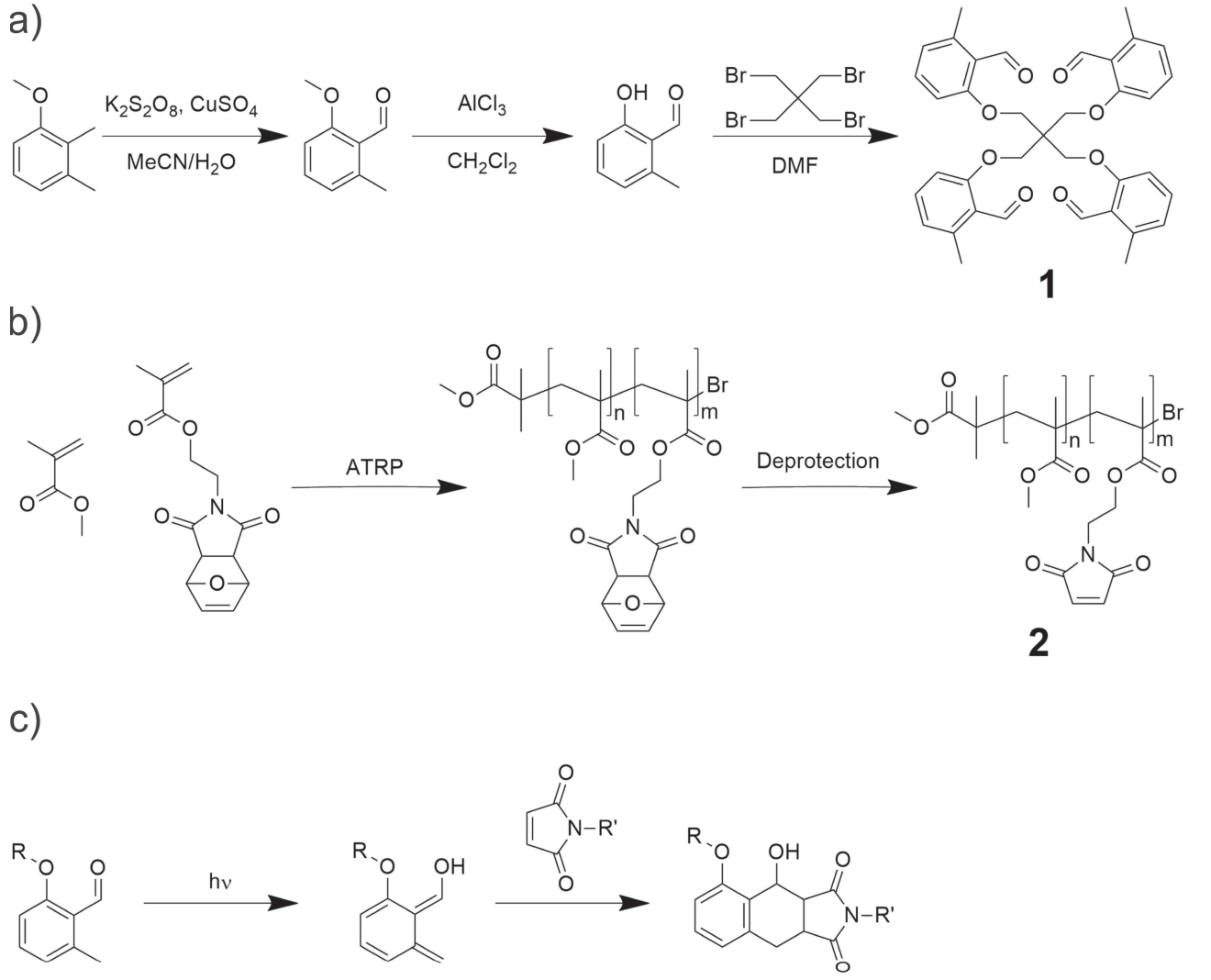

Figure 2. a) and b) depict the synthetic pathways for the generation of the reactive compounds **1** and **2**, respectively. c) Depicts the photo-induced *o*-quinodimethane generation and the reaction of this intermediate species with a maleimide functional group to form the Diels–Alder cycloproduct.

reactions are prevented from taking place during or after the fabrication process as the reaction product is energetically stabilized due to the reformation of the aromatic system. By combining compound **1** and **2** in the photoresist, 3D microstructures can be fabricated utilizing femtosecond pulses centered around 700 nm wavelength. The selected wavelength ensures an efficient multiphoton absorption by compound **1** (for UV-VIS see Figure S1c, Supporting Information, for two-photon absorption sensitivity compare [12]) and can be conveniently delivered by a single-box turn-key tunable Ti:sapphire laser oscillator.

An important parameter is the extent of reaction that is necessary for the formation of insoluble material for the employed compounds. For step polymerizations performed with multifunctional monomers, calculation of the gel point which can be defined as the point where an insoluble polymer fraction is formed is possible.[36] For the given system assuming, stoichiometric amounts of reactants, the fraction of functional groups that must have reacted in order to reach the gel point was calculated to be 33%. After gelation of an exposed area, a soluble fraction consisting of monomer, oligomers, polymer chains and solvent remains. The polymerization continues beyond the gel point, increasing the amount of gel while decreasing the amount of soluble fraction for progressing conversion. Therefore, the calculated critical extent of reaction should rather be seen as a minimum value for conversions that are obtained during DLW. In sharp contrast to step polymerizations, the gel point in CPs (e.g., free radical polymerization of multifunctional monomers) occurs at much lower conversions. As an example, the addition of small amounts of divinyl benzene to styrene polymerizations drastically decreases the conversion at which gelation occurs to about 5% for a divinyl benzene content of 20 wt%.[37] Presumably, the gel point for bulk polymerization of multifunctional acrylates commonly employed for DLW even lies below this value. It is therefore assumed that non-radical step polymerization based photoresists require larger conversions for solid network material generation. Therefore, the here selected crosslinking reaction must occur very rapid and efficient.

The proper choice of solvent is another important issue. To avoid evaporation of the solvent and resulting changes in reagent concentration, we chose γ-butyrolactone (GBL) and acetophenone as a low-volatility solvent mixture. During the DLW experiments performed in this study (typically up to six hours), only minor evaporation-related shifts in the threshold power were observed. The two solvent system was chosen as each solvent efficiently dissolves one active component of the resist, allowing for a total content of active material in the resist of close to 9.5 wt%.

4. Fabrication and Characterization of Woodpile Photonic Crystals

An important parameter for every DLW system is the resolution that can be obtained for 3D structures. In order to facilitate the comparison between different systems, woodpile photonic crystals are often employed as benchmark structures for the determination of the achievable resolution.[21] Woodpile photonic crystals are 3D objects that exhibit photonic stop bands.[10,38] The spectral location of these stop bands is dependent on parameters such as the rod to rod spacing and the distance between layers. SEM images of a woodpile photonic crystal generated via multiphoton induced Diels–Alder chemistry are depicted in **Figure 3**. The structure consists of a total of 20 layers (5 periods) with a rod spacing of 700 nm, a layer distance of close to 250 nm and a 20 μm × 20 μm footprint with writing conditions of 4.3 mW average laser power and 100 μm s^{-1} writing speed. The interior of the structure is revealed by focused ion beam milling, demonstrating that the targeted architecture has been achieved throughout the entire structure. An alternative way to monitor the quality of the woodpile structures is by spectral analysis of the corresponding photonic stop bands. For this purpose, an array of woodpile photonic crystals was fabricated allowing for the variation of the rod spacing (also affecting the layer to layer distance) and the exposure power. The rod spacing was varied between 700 nm and 500 nm, and the laser power was varied between 2.7 mW and 3.6 mW with a writing speed of 100 μm s^{-1}. Such an array enabled the determination of optimal fabrication conditions for structures with different rod spacing. For rod spacing well below 1 μm, the corresponding photonic stop band is found in the visible light spectrum. Transmission and reflection spectra of selected woodpile photonic crystals with a rod spacing between 700 nm and 600 nm are depicted in **Figure 4**a, revealing a stop band in the visible for each rod spacing. The photonic stop bands are, as expected, clearly shifted to lower wavelengths for decreased rod spacing. Stop bands of intact photonic crystals in the visible range can also be readily identified by their color in light microscope imaging, as depicted in Figure 4b. Here, woodpile structures with a rod spacing between 600 nm and 500 nm are shown. While a range of different excitation powers yield intact photonic crystals with 600 nm and 550 nm rod spacing, the power range as well as the quality of the produced structure has decreased considerably for structures with 500 nm rod spacing, marking the achievable resolution for this particular resist.

We see several distinct differences of the system presented here as compared to resists employed in the literature such as cationic polymerization of SU8, radical thiol-ene polymerization or radical polymerization of multifunctional acrylates. The effect of shrinkage during development of the sample usually becomes less pronounced for structures that are far from the resolution limit utilizing, for example, radical acrylate polymerization. For 700 nm woodpile photonic crystal presented in this study, shrinkage is still clearly visible. A possible explanation for this behavior is the difference in crosslinking density that can be achieved in both systems. The employed copolymer with a molecular weight of 10 500 Da exhibits 12 maleimide functional groups, entailing a maximum of 12 crosslinks per polymer chain. For comparison, a linear fragment of the crosslinked polymer gained from pentaerythritol triacrylate with equal molecular weight would exhibit close to 70 acrylate groups, allowing for a much higher crosslinking density. High crosslinking densities decrease the flexibility of the network and thus impede distortion of the material after curing. The photoenol mediated structures presented here also exhibit a certain surface roughness which may occur due to the relatively low monomer content in the resist (9.5 wt% for the photoenol resist, close to 90%wt triacrylate content for a typical bulk free radical polymerization). Both shrinkage and surface roughness are adverse for the fabrication of photonic crystals as they lead to disturbance of the required periodicity. Nevertheless, woodpile photonic crystals have been fabricated with visible photonic stop bands for rod spacing of down to 500 nm. While conventional radical acrylate polymerization provides even higher resolution with rod spacing of down to 400 nm,[21] the here achieved parameters are well below any woodpile photonic crystals fabricated via cationic polymerization of SU8 (650 nm

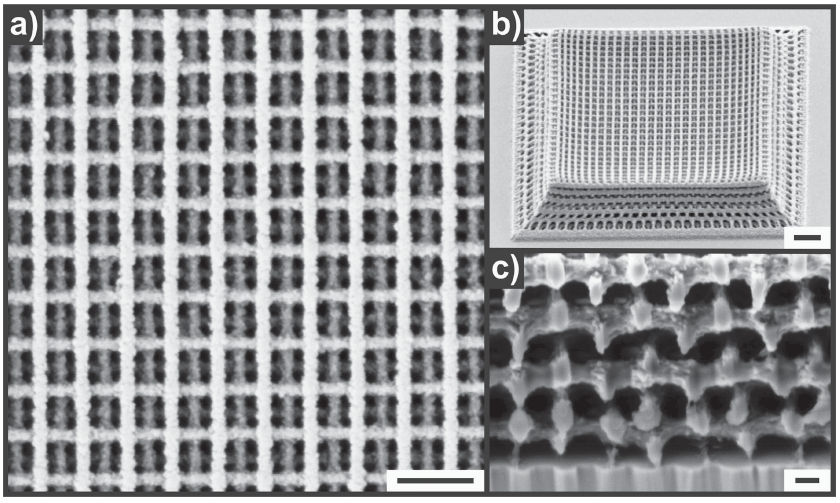

Figure 3. SEM images of a woodpile photonic crystal fabricated via multiphoton-induced Diels–Alder chemistry with a lateral rod spacing of 700 nm. A closeup top view is depicted in a) whereas b) shows the entire fabricated structure. c) Depicts the interior of the woodpile after focused ion beam milling. Scale bars are 1 μm, 2 μm, and 200 nm, respectively.

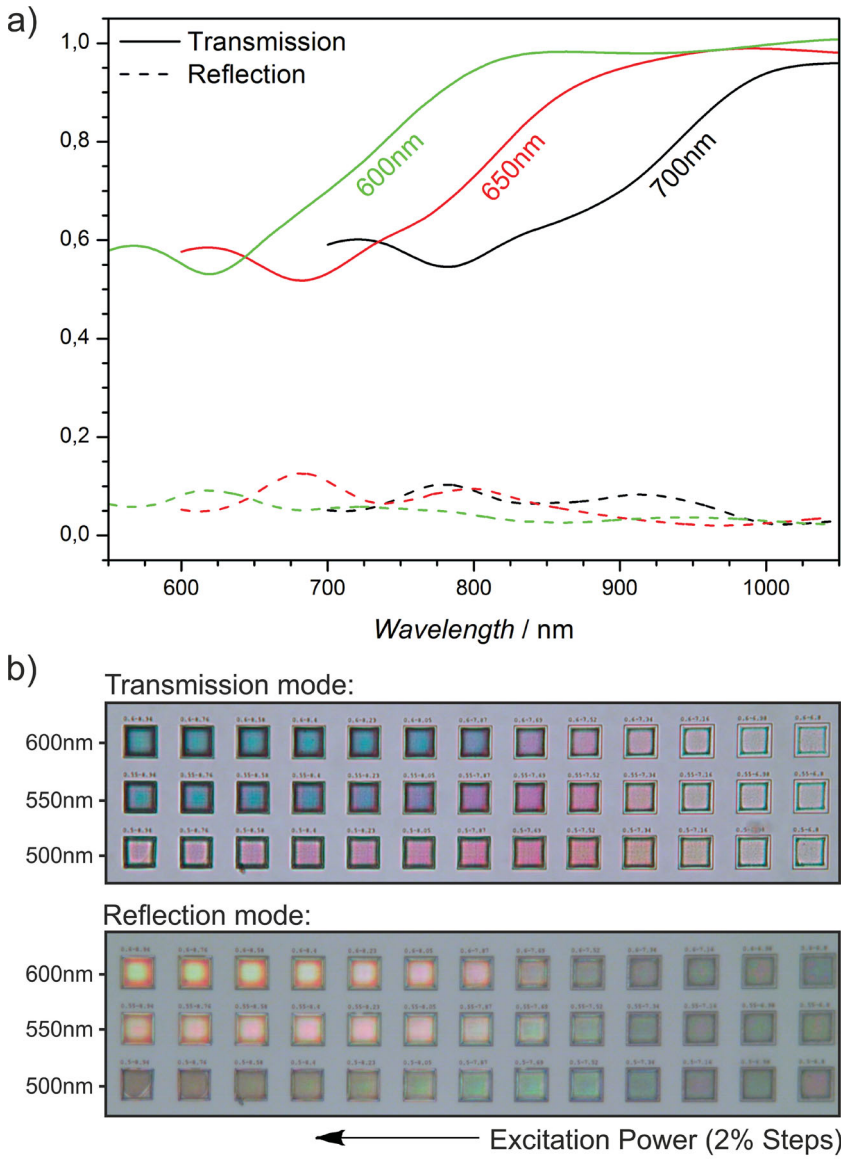

Figure 4. a) Transmission and reflection spectra of woodpile photonic crystals with rod spacing varying from 700 nm to 600 nm. b) Light microscope images in transmission and reflection mode of woodpile photonic crystals written at different laser powers with rod spacing varying from 600 nm to 500 nm.

rod spacing)[10] or radical thiol-ene polymerization (2 µm rod spacing).[25]

5. Chemical Analysis of Fabricated Polymer Structures

After determination of the resolution limits for the here presented resist, it is important to verify that the Diels–Alder reaction is actually responsible for the formation of insoluble network material during DLW. Theoretically, every component of the resist could undergo unwanted side reactions. In order to exclude that the solubility change during DLW stems from reactions of a single active component with itself and/or the solvent mixture, several blind test resists were produced and tested in the DLW system (see Table S1, Supporting Information). The test resists consisted of up to one single active compound and the solvent mixture. They were cured in the DLW setup under identical fabrication conditions employed for the original resist. For each test resist, no solubility change was observed, even at significantly larger average laser powers (up to 10 mW) than utilized for structure fabrication with the original resist containing both compounds **1** and **2** (≈3 mW). The blind tests reveal that the reaction which is responsible for the solubility change requires both active components to be present in the resist. However, this simple analysis provides no information about the nature of the crosslinking reaction.

In order to evidence the occurrence of the Diels–Alder reaction, FTIR spectra of each active compound (compound **1** and **2**), their stoichiometric mixture (concerning the number of maleimide and aldehyde functional groups) and a fabricated microstructure were recorded and compared (see **Figure 5**). The microstructure is a solid polymeric block with a footprint of 50 µm × 50 µm and an approximate height of 10 µm. For the single active compounds and the stoichiometric mixture (without solvent) attenuated total reflection IR was performed while transmission IR was conducted for microstructure analysis.[39] Compound **1** contains an aldehyde functional group with an absorption band clearly visible at 1680 cm^{-1} corresponding to the stretching vibration of the carbonyl group. Another specific absorption band of the aldehyde can be identified at 2780 cm^{-1} stemming from the Fermi-Resonance of the C–H stretching vibration and the first overtone of the deformation vibration of H–C=O. The second absorption band arising from the Fermi-Resonance is located at approximately 2890 cm^{-1} and is not further considered as the weak signal overlaps with other absorption bands. Compound **2** contains two ester groups and an unsaturated imide within the polymer repeating units. The strong absorption band at 1700 cm^{-1} stems from the stretching vibration of both ester groups and the unsaturated imide of the comonomer. The visible shoulder situated at 1730 cm^{-1} is assigned to the remaining imide group of the comonomer, as the absorption bands corresponding to imides typically consist of two peaks. FTIR analysis of the stoichiometric mixture of both components (1+2) reveals that all absorption bands that have been assigned to the different carbonyl groups remain clearly visible in the spectrum. During the photoenolization process, the reactive *o*-quinodimethane species is formed which subsequently undergoes a Diels–Alder reaction with

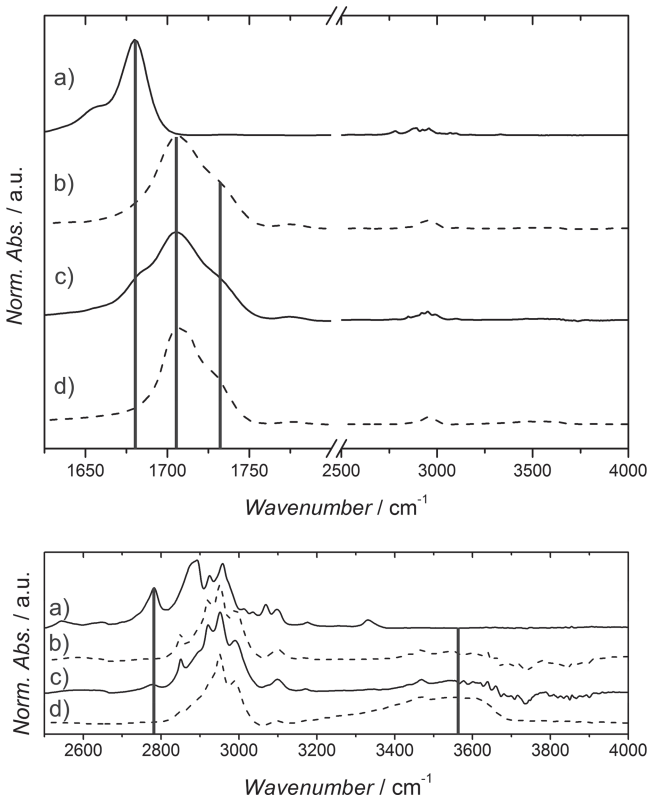

Figure 5. Top: FTIR spectra of a) **1**, b) **2**, c) a stoichiometric mixture of **1** and **2**, and d) a microstructure fabricated via DLW. Bottom: enlarged depiction of the spectra in the range of 2500–4000 cm^{-1}. The spectra clearly show that absorption peaks at 1680 cm^{-1} and 2780 cm^{-1} corresponding to the aldehyde group of **1** disappear during structure fabrication, whereas absorption peaks corresponding to the ester and imide groups of **2,** situated at 1700 cm^{-1} and 1730 cm^{-1} remain after exposure. Furthermore, a broad peak at 3200–3700 cm^{-1} appears in (d) that can be assigned to the hydroxyl group formed during fabrication. For better readability, the spectra are shifted vertically.

the provided maleimide. Thereby, aldehyde functional groups are consumed and hydroxyl groups are generated. This process can be evidenced by the FTIR measurement of the microstructure. Absorption peaks corresponding to aldehyde functional groups at 1680 cm^{-1} and 2782 cm^{-1} that are clearly visible in the stoichiometric mixture (1+2) are not present in the spectrum of the microstructure. All absorption peaks corresponding to the remaining carbonyl groups of the active compounds remain visible in the spectrum. This is expected as apart from the change in saturation of the imide which has no large influence on the position of the absorption band, no other carbonyl group is altered during reaction. Furthermore, a broad absorption peak in the range of 3200–3700 cm^{-1} appears in the spectrum that can be assigned to the formed hydroxyl group. The here discussed results clearly evidence that the photo-induced Diels–Alder reaction is responsible for the solubility change in the exposed area of the photoresist, thereby also revealing that photoenolization of compound **1** can be efficiently triggered via multiphoton absorption (consistent with the literature).[12]

6. Spatially Resolved Surface Modification

Having verified the polymerization reaction in the preceding section, the following section focuses on covalent surface modification of prepared microstructures. To date, covalent functionalization reactions on DLW fabricated structures have been performed via thiol-Michael addition reactions[25] and Diels–Alder chemistry.[12] The latter method has been employed for spatially resolved surface modification, yet the corresponding procedure requires multiple reaction steps as well as dedicated fabrication and functionalization setups. A simple protocol allowing for spatially resolved functional structures is therefore of high interest. During the fabrication of 3D structures via the here presented system, a large fraction of the participating reactive groups is consumed. However, due to the decrease in mobility of the reactants with increasing conversion, full conversion is not achieved during solid network material generation. Thus, reactive groups remain throughout the written structure, some of which are located on the structures surface. These accessible residual functional groups can be addressed for direct modification of the polymer surface of a developed sample. By immersing the sample in a solution of maleimide-containing functional molecules, the light induced Diels–Alder reaction can be employed for covalent surface patterning. It can be assumed that the conditions for both the patterning and the fabrication reaction are similar as both the reaction and the participating functional groups are identical. Therefore, the DLW fabrication setup can also be employed for post fabrication patterning purposes, allowing for a spatially resolved modification reaction in selected surface areas. Within the scanned areas, reactive *o*-quinodimethane moieties are generated from corresponding precursor molecules located on the surface that can readily react via the Diels–Alder reaction (see **Figure 6**a). As a demonstration, the bromine containing compound **3** in solution is covalently bonded to the exposed surface areas. A potential side reaction between the *o*-quinodimethane species and residual maleimides arising from the fabrication process is impeded due to the low mobility of both species. ToF-SIMS measurements of structures spatially functionalized with compound **3** are depicted in Figure 6b. The fabricated structure is a massive polymer block with a footprint of 90 µm × 90 µm and a height of close to 300 nm. Onto the surface of this structure, the Karlsruhe Institute of Technology logo with a total footprint of approximately 60 µm × 40 µm was patterned employing the DLW setup. Throughout the exposed area, the amount of bromine detected by signals corresponding to each isotope (79.16 u and 81.17 u) is drastically increased, providing strong evidence for the covalent attachment of compound **3** to the targeted surface area. By close examination of the presented ToF-SIMS images, it becomes apparent that a small quantity of bromine is also present throughout the unexposed surface of the structures. However, this signal is not assigned to unwanted covalent attachment or adhesion of compound **3**. It rather stems from the bromine groups present in compound **2** (generated via atom transfer radical polymerization), incorporated throughout the structure during the fabrication step. In the current work a bromine containing maleimide was employed for surface modification as it allows for an easy and

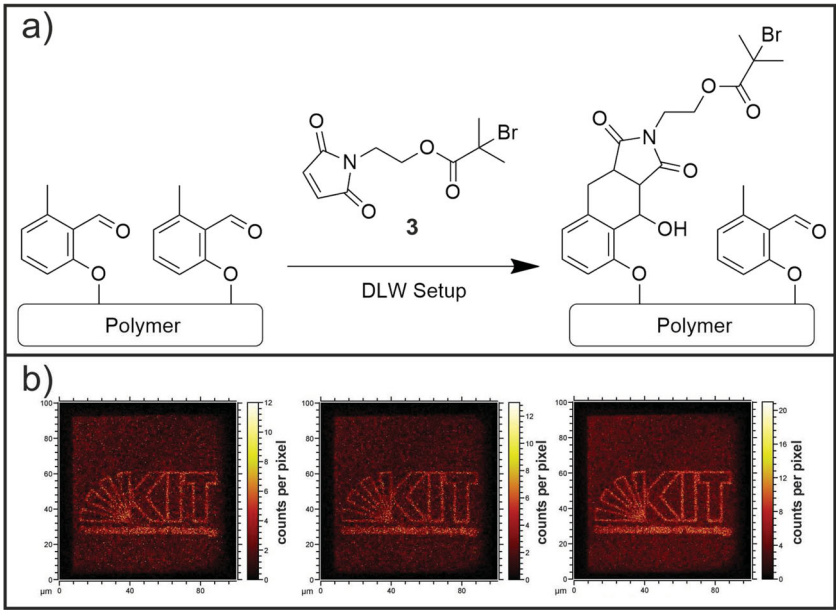

Figure 6. a) Light-induced Diels–Alder reaction between residual *o*-quinodimethane precursor molecules on fabricated structures and bromine containing maleimides (compound **3**) in solution. Employing the DLW setup allows for spatial surface modification as the reaction only takes place in exposed areas. b) ToF-SIMS images of ^{79}Br, ^{81}Br, and their sum (from left to right). The area scanned with the DLW setup is clearly visible as it contains an increased amount of covalently bound bromine.

distinct determination via ToF-SIMS. However, this system is not restricted to one compound. Essentially any molecule that is inert to 700 nm light exposure and contains a reactive dienophile can be covalently bonded to exposed areas of the structure, making the introduced technique highly promising for future applications. It is furthermore emphasized that the here presented technique allows for the fabrication and direct functional surface patterning of 3D microstructures utilizing one single lithographic setup and one single reaction for both the fabrication and the patterning step.

7. Conclusion

The successful fabrication of 3D microstructures was demonstrated by combining DLW and a non-radical step polymerization based on multiphoton-induced Diels–Alder chemistry. Woodpile photonic crystals with a rod spacing ranging from 700 nm to 500 nm were fabricated and the structure quality was investigated via SEM, focused ion beam milling, transmission and reflection spectroscopy as well as light microscopy. Furthermore, FTIR analysis verified that the Diels–Alder reaction is responsible for the generation of the crosslinked material during structure fabrication. A highly important feature of the novel system is—contrary to established radical or cationic polymerization protocols—the possibility for direct, rapid and facile spatial surface modification after structure fabrication. For arbitrary surface patterning the photo-induced Diels–Alder reaction was again utilized in combination with the DLW setup. Successful surface modification was demonstrated utilizing a bromine containing maleimide, yet the presented system is in principle compatible with any light stable, reactive dienophile. The achievable resolution combined with direct patterning of the here presented technique may prove to be particularly useful, for example, for the attachment of cell signaling molecules in the context of advanced cell behavior studies or a cascade of microreactors in microfuidic lab-on-a-chip systems.

8. Experimental Section

Materials: GBL (≥99%, Sigma Aldrich), acetophenone (99%, Sigma Aldrich), pentaerythritol tetrabromide (96%, Sigma Aldrich), dimethylformamide (DMF, 99.5%, Acros Organics), potassium carbonate (K_2CO_3, ≥99%, Roth), acetonitrile (anhydrous, Fischer), dichloromethane (analytical grade, Fischer), hexane (analytical grade, Prolabo), ethyl acetate (analytical grade, Prolabo), basic alumina oxide (VWR), diethyl ether (Et_2O, analytical grade, Prolabo), isopropanol (≥99.5%, Roth), tetrahydrofuran (THF, GPC-grade, VWR), methyl α-bromoisobutyrate (≥99%, Sigma Aldrich), *N*, *N*, *N′*, *N″*, *N″*-pentamethyldiethylenetriamine (PMDETA, 99+%, Acros Organics), copper(II) bromide (99%, Sigma Aldrich), methanol (MeOH, analytical grade, VWR) and toluene (analytical grade, Prolabo) were used without further treatment. Acetone (99.5%, Roth) employed for atom transfer radical polymerization was dried over sodium sulfate prior to usage. Methyl methacrylate (99+%, Acros Organics) was deinhibited by percolating over a column of basic alumina oxide and stored at –19 °C prior to usage. CuBr (98%, Sigma Aldrich) was successively washed with acetic acid and Et_2O and dried under vacuum.[40]

Synthesis of 2-hydroxy-6-methylbenzaldehyde: 2-hydroxy-6-methylbenzaldehyde was synthesized employing a literature procedure.[41]

Synthesis of 6,6′-((2,2-bis((2-formyl-3-methylphenoxy)methyl) propane-1,3-diyl)bis(oxy))bis(2-methylbenzaldehyde) (**1**): 2-Hydroxy-6-methylbenzaldehyde (1.30 g, 9.56 mmol, 7 eq), pentaerythritol tetrabromide (0.53 g, 1.37 mmol, 1 eq) and K_2CO_3 (2.83 g, 20.48 mmol, 15 eq) was dissolved in 45 mL of DMF in a 100 mL round bottom flask, equipped with a stir bar and a reflux condenser. The reaction mixture was heated to 120 °C and stirred for 3 days. The now black reaction solution was subsequently allowed to cool to ambient temperature. Thereafter, the solvent was removed under reduced pressure at 80°C. Then, silica gel (~10 g) and 40 mL of acetonitrile/dichloromethane (7:3) was added to the black residue. After removing the solvent under reduced pressure, the crude product was further purified via column chromatography (hexane:ethyl acetate, 7:3, r_f = 0.4) to give a yellow solid. The yellow solid was excessively washed with Et_2O to yield the final product as an off-white powder that was dried in vacuo at 50 °C. Yield: 0.41 g, 50%. ^1H NMR (400 MHz, $CDCl_3$, δ): 10.61 (s, 4H; CHO), 7.38 (t, *J* = 8.0 Hz, 4H; ArH), 6.89 (d, *J* = 8.4 Hz, 4H, ArH), 6.83 (d, *J* = 7.6 Hz, 4H, ArH), 4.50 (s, 8H; CH_2), 2.54 (s, 12H, CH_3); ^{13}C NMR (100 MHz, $CDCl_3$, δ): 190.9 (CHO), 161.4 (OCAr), 142.6 (CH_3CAr), 135.0 (CAr), 125.0 (CAr), 123.5 (CHCAr), 110.2 (CAr), 67.0 (CH_2), 45.8 ($C(CH_2O)_4$), 21.2 (CH_3).

Synthesis of 2-(1,3-dioxo-3a,4,7,7a-tetrahydro-1H-4,7-epoxyisoindol-2(3H)-yl)ethyl methacrylate: 2-(1,3-dioxo-3a,4,7,7a-tetrahydro-1H-4,7-epoxyisoindol-2(3H)-yl)ethyl methacrylate was synthesized employing a literature procedure.[35]

Synthesis of poly [(methyl methacrylate)-co-(2-(2,5-dioxo-2,5-dihydro-1H-pyrrol-1-yl)ethyl methacrylate)] (**2**): A 25 mL schlenk flask was equipped

with methyl methacrylate (3.5 mL, 3.3 g, 32.9 mmol, 4.1 eq), 2-(1,3-dioxo-3a,4,7,7a-tetrahydro-1H-4,7-epoxyisoindol-2(3H)-yl)ethyl methacrylate (2.2 g, 7.9 mmol, 1.0 eq), methyl α-bromoisobutyrate (52.0 µL, 72.8 mg, 0.4 mmol, 0.05 eq), PMDETA (52.0 µL, 43.2 mg, 0.25 mmol, 0.03 eq), $CuBr_2$ (4.0 mg, 0.02 mmol, 0.002 eq) 4 mL of acetone and a stir bar. Three consecutive freeze-pump-thaw cycles were performed. To the still frozen reaction mixture CuBr (16.0 mg, 0.11 mmol, 0.014 eq) was added under reverse flow of nitrogen. After two additional consecutive freeze-pump-thaw cycles, the flask was rapidly heated to 50 °C in a preheated oil bath and stirred for 7.5 h. The reaction solution was subsequently exposed to air and passed through a short column of neutral alumina oxide. The generated polymer was precipitated in cold MeOH. The precipitated polymer was then dissolved in 15 mL of toluene in a 25 mL round bottom flask which was then connected to a condenser. The reaction mixture was then heated to reflux for 24 h. Furan and solvent were removed under reduced pressure. The solid residue was dissolved in toluene and precipitated in cold MeOH. The Product was dried under reduced pressure at 50 °C to yield a white solid (1.5 g). SEC: M_n = 10500 Da, PDI = 1.2; ^{1}H NMR (400 MHz, $CDCl_3$, δ): 6.80 (s, 2H; CH(C = O)N), 4.03 (s, 2H, H_2CO), 3.80 (s, 2H, H_2CN), 3.57 (s, 3H, H_3CO), 2.03-1.66 (m, 2H, CCH_2C), 1.05-0.66 (m, 3H, CH_3C). For the calculation of the number of maleimide groups per polymer chain, the integrals of the ^{1}H-NMR signals at 6.80 ppm and 3.57 ppm as well as the M_n of the SEC measurement where employed. The number of maleimide groups per polymer molecule was calculated to be close to 12.

Synthesis of 2-bromo-2-methyl propionic acid 2-(3,5-dioxo-10-oxa-4-azatricyclo[5.2.1.02,6]dec-8-en-4-yl) ethyl ester (**3**): 2-bromo-2-methyl propionic acid 2-(3,5-dioxo-10-oxa-4- azatricyclo[5.2.1.02,6]dec-8-en-4-yl) ethyl ester was synthesized employing a literature procedure.[42]

Synthesis of N-(3-(trimethoxysilyl)propyl)acrylamide: N-(3-(trimethoxysilyl)propyl) acrylamide was synthesized employing a literature procedure.[43]

^{1}H and ^{13}C Nuclear Magnetic Resonance Spectroscopy: ^{1}H and ^{13}C NMR spectroscopy performed using a Bruker AM 400 spectrometer at 400 MHz. All samples were dissolved in $CDCl_3$. The δ-scale is referenced to the internal standard tetramethylsilane (TMS, δ = 0.00 ppm).

Size Exclusion Chromatography: Size Exclusion chromatography was performed using a Polymer Laboratories PL-GPC 50 Plus system, comprised of an auto injector, a guard column (PLgel Mixed C, 50 × 75 mm) followed by three linear columns (PLger Mixed C, 300 × 7.5 mm, 5 µm bead size) and a differential refractive index detector, was employed. THF at 40 °C at a flow rate of 1 mL min^{-1} was used as the eluent. The GPC system was calibrated using narrow poly(methyl methacrylate) standards ranging from 600 to 5195 g mol^{-1} (Polymer Standards Service (PSS), Mainz, Germany). The resulting molar mass distributions were determined by universal calibration using Mark-Houwink parameters for PMMA (K = 12.8 10^{-5} dL g^{-1}, α = 0.69). All M_n values were calculated using a PMMA calibration curve and the Mark-Houwink correction parameters, K and α.

UV-VIS Measurements: UV-VIS Measurements were recorded on a Varian Cary 300 Bio spectrophotometer.

Infrared Spectroscopy: Infrared spectroscopy measurements were performed on a Fourier-transform microscope spectrometer (Bruker Tensor 27 with Hyperion 1000 unit). Spectra of compound **1**, compound **2** and the stoichiometric mixture of **1** and **2** were measured using attenuated total reflection infrared spectroscopy. The microstructure was characterized via transmission IR spectroscopy using the Hyperion 1000 unit. Atmospheric compensation and baseline correction was performed upon the obtained spectra. The spectra were normalized via the highest carbonyl absorption band at 1680–1710 cm^{-1}.

Scanning Electron Microscopy: SEM images were recorded using a Zeiss Supra 40VP. All samples were coated with a 10 nm gold layer prior to measurements.

Focussed Ion Beam Milling: Focussed ion milling was performed using a Zeiss Auriga equipped with a gallium ion source. The applied current was set to be 50 pA/30 kV. All samples were coated with a 10 nm gold layer prior to measurements.

Transmission and Reflection Spectra: Transmission and reflection spectra of the woodpile photonic crystals were taken using a commercial FTIR-spectrometer-microscope (Bruker Equinox 55). The Cassegrain objective (Opticon 36x, NA = 0.5) used illuminates the sample in the angular interval 15°–30° from the optical axis.

Time-of-Flight Secondary Ion Mass Spectrometry: Time-of-flight secondary ion mass spectrometry was performed on a TOF.SIMS5 instrument (ION-TOF GmbH, Münster, Germany), equipped with a Bi cluster primary ion source and a reflectron type time-of-flight analyzer. UHV base pressure was < 5 × 10^{-9} mbar. For high mass resolution the Bi source was operated in the "high current bunched" mode providing short Bi_1^+ or Bi_3^+ primary ion pulses at 25 keV energy and a lateral resolution of approx. 4 µm. The short pulse length of 1.1 ns allowed for high mass resolution. Spectra were calibrated on the omnipresent C^-,CH^-, CH_2^-, C_2^-, C_3^-, or on the C^+, CH^+, CH_2^+, and CH_3^+ peaks. ^{79}Br and ^{81}Br peaks were not accompanied by other strong peaks at identical nominal masses; therefore, for high lateral resolution imaging the primary ion source was operated in "burst alignment" mode. Here, only nominal mass resolution is obtained but the lateral resolution of the instrument is in the range of 150 nm. Images of 256 × 256 pixel were recorded, no filtering/averaging was performed.

Direct Laser Writing Experiments: Direct laser writing experiments were conducted using a home-built setup that has been previously described in detail.[44] The pulse-picker described in the reference has been removed resulting in a repetition rate of 80 MHz and the laser has been tuned to 700 nm center wavelength.

Photoresist Preparation: The resist employed for photoenol mediated DLW experiments consists of 6,6'-((2,2-bis((2-formyl-3-methylphenoxy)methyl)propane-1,3-diyl)bis(oxy))bis(2-methylbenzaldehyde) (**1**) (5 mg, 8.2 × 10^{-6} mol), poly [(methyl methacrylate)-co-(2-(2,5-dioxo-2,5-dihydro-1H-pyrrol-1-yl)ethyl methacrylate)] (**2**) (29.2 mg, 8.2 × 10^{-6} mol), 150 µL of GBL and 150 µL of acetophenone. After dissolving of the solid compounds, the resist was passed through a filter (Whatman, Spartan 13/0.2 RC).

Preparation of Glass Substrates: All glass substrates were cleaned by ultrasonification for 15 min in acetone. Preactivation of the surfaces was achieved by exposure to air plasma for 10 min. Preactivated glass substrates were placed separately in small glass vials containing a solution of N-(3-(trimethoxysilyl)propyl) acrylamide dissolved in toluene (1 10^{-3} mol L^{-1}) for 60 min at ambient temperature without stirring. The substrates were successively ultrasonicated in toluene (10 mL, 10 min) and acetone (10 mL, 5 min) to remove any physisorbed silane. The silanization process is performed in order to covalently bind the fabricated structures to the substrate surface during fabrication. The adhesive strength is thereby increased.

DLW Sample Preparation and Development: DLW samples were prepared and developed according to a literature procedure.[25]

Fabrication of Woodpile Photonic Crystals: Woodpile photonic crystals with rod spacings ranging from 700 nm to 500 nm were fabricated. The average laser power was varied between 2.7 mW and 4.3 mW. The writing speed was set to be 100 µm s^{-1}.

DLW Samples for IR Spectroscopy: A solid polymer block was fabricated exhibiting a footprint of 50 µm × 50 µm and a height of close to 10 µm for characterization via IR spectroscopy. The laser power and the writing speed were set to be 5 mW and 100 µm s^{-1}, respectively.

DLW Samples for Spatial Surface Patterning: Solid polymer blocks with base dimensions of 90 µm × 90 µm and a height of about 300 nm were fabricated. The fabrication parameters were set to be 5 mW average laser power and 100 µm s^{-1} writing speed.

Spatial Surface Patterning: DLW fabricated structures were immersed into a solution of 2-bromo-2-methyl propionic acid 2-(3,5-dioxo-10-oxa-4-azatricyclo[5.2.1.02,6]dec-8-en-4-yl) ethyl ester in DMF (3 mg mL^{-1}) much similar to the preparation of a common DLW sample. Patterning was conducted using the DLW setup with fabrication parameters of 5 mW average laser power and 10 µm s^{-1} writing speed. Sample development was performed by immersing the sample into DMF (30 mL, 2h) and subsequent rinsing with acetone (5 mL), isopropanole

(5 mL) and distilled water (5 mL). Residual solvent was removed under reduced pressure.

Supporting Information

Supporting Information is available from the Wiley Online Library or from the author.

Acknowledgements

The authors acknowledge Patrice Brenner for performing focused ion beam milling, Johannes Kaschke for scanning electron microscopy measurements and Michael Thiel for the generation of the microscopic KIT logo. C.B.-K. acknowledges continued support from the Karlsruhe Institute of Technology (KIT) via the STN Helmholtz program. M.W. achnowledges support by the Karlsruhe Institute of Technology (KIT) through the DFG Center for Functional Nanostructures (CFN). The PhD education of B.R. is embedded in the Karlsruhe School of Optics & Photonics (KSOP).

Received: November 30, 2013
Revised: January 14, 2014
Published online: March 10, 2014

[1] Y. Chen, A. Pépin, *ELECTROPHORESIS* **2001**, *22*, 187–207.
[2] L. J. Guo, *Adv. Mater.* **2007**, *19*, 495–513.
[3] G. Subramania, Y.-J. Lee, I. Brener, T.-S. Luk, P. G. Clem, *Opt. Express* **2007**, *15*, 13049–13057.
[4] C. N. LaFratta, J. T. Fourkas, T. Baldacchini, R. A. Farrer, *Angew. Chem. Int. Ed.* **2007**, *46*, 6238–6258.
[5] S. Maruo, J. T. Fourkas, *Laser Photonics Rev.* **2008**, *2*, 100–111.
[6] M. Malinauskas, M. Farsari, A. Piskarskas, S. Juodkazis, *Phys. Rep.* **2013**, *533*, 1–31.
[7] T. G. Leong, A. M. Zarafshar, D. H. Gracias, *Small* **2010**, *6*, 792–806.
[8] S. Maruo, K. Ikuta, H. Korogi, *Appl. Phys. Lett.* **2003**, *82*, 133–135.
[9] S. Klein, A. Barsella, H. Leblond, H. Bulou, A. Fort, C. Andraud, G. Lemercier, J. C. Mulatier, K. Dorkenoo, *Appl. Phys. Lett.* **2005**, *86*, 211118–211113.
[10] M. Deubel, G. von Freymann, M. Wegener, S. Pereira, K. Busch, C. M. Soukoulis, *Nat. Mater.* **2004**, *3*, 444–447.
[11] K. K. Seet, V. Mizeikis, S. Matsuo, S. Juodkazis, H. Misawa, *Adv. Mater.* **2005**, *17*, 541–545.
[12] B. Richter, T. Pauloehrl, J. Kaschke, D. Fichtner, J. Fischer, A. M. Greiner, D. Wedlich, M. Wegener, G. Delaittre, C. Barner-Kowollik, M. Bastmeyer, *Adv. Mater.* **2013**, *25*, 6117–6122.
[13] F. Klein, T. Striebel, J. Fischer, Z. Jiang, C. M. Franz, G. von Freymann, M. Wegener, M. Bastmeyer, *Adv. Mater.* **2010**, *22*, 868–871.
[14] A. W. Schell, J. Kaschke, J. Fischer, R. Henze, J. Wolters, M. Wegener, O. Benson, *Sci. Rep.* **2013**, *3*, 1577.
[15] B.-B. Xu, Y.-L. Zhang, H. Xia, W.-F. Dong, H. Ding, H.-B. Sun, *Lab on a Chip* **2013**, *13*, 1677–1690.
[16] M. Malinauskas, P. Danilevičius, S. Juodkazis, *Opt. Express* **2011**, *19*, 5602–5610.
[17] M. Thiel, J. Fischer, G. von Freymann, M. Wegener, *Appl. Phys. Lett.* **2010**, *97*, 221102.
[18] K. Cicha, Z. Li, K. Stadlmann, A. Ovsianikov, R. Markut-Kohl, R. Liska, J. Stampfl, *J. Appl. Phys.* **2011**, *110*, 064911–064915.
[19] N. Pucher, A. Rosspeintner, V. Satzinger, V. Schmidt, G. Gescheidt, J. Stampfl, R. Liska, *Macromolecules* **2009**, *42*, 6519–6528.
[20] Z. Li, N. Pucher, K. Cicha, J. Torgersen, S. C. Ligon, A. Ajami, W. Husinsky, A. Rosspeintner, E. Vauthey, S. Naumov, T. Scherzer, J. Stampfl, R. Liska, *Macromolecules* **2013**, *46*, 352–361.
[21] J. Fischer, M. Wegener, *Opt. Mater. Express* **2011**, *1*, 614–624.
[22] A. Ovsianikov, J. Viertl, B. Chichkov, M. Oubaha, B. MacCraith, I. Sakellari, A. Giakoumaki, D. Gray, M. Vamvakaki, M. Farsari, C. Fotakis, *ACS Nano* **2008**, *2*, 2257–2262.
[23] M. Farsari, B. N. Chichkov, *Nat. Photonics* **2009**, *3*, 450–452.
[24] E. Kabouraki, A. N. Giakoumaki, P. Danilevicius, D. Gray, M. Vamvakaki, M. Farsari, *Nano Lett.* **2013**, *13*, 3831–3835.
[25] A. S. Quick, J. Fischer, B. Richter, T. Pauloehrl, V. Trouillet, M. Wegener, C. Barner-Kowollik, *Macromol. Rapid Comm.* **2013**, *34*, 335–340.
[26] B. J. Adzima, C. J. Kloxin, C. A. DeForest, K. S. Anseth, C. N. Bowman, *Macromol. Rapid Comm.* **2012**, *33,*2092–2096.
[27] H. C. Kolb, M. G. Finn, K. B. Sharpless, *Angew. Chem. Int. Ed.* **2001**, *40*, 2004–2021.
[28] J. Fischer, M. Wegener, *Laser Photonics Rev.* **2012**, *7*, 22–44.
[29] C. Barner-Kowollik, F. E. Du Prez, P. Espeel, C. J. Hawker, T. Junkers, H. Schlaad, W. Van Camp, *Angew. Chem. Int. Ed.* **2011**, *50*, 60–62.
[30] P. G. Sammes, *Tetrahedron* **1976**, *32*, 405–422.
[31] J. L. Segura, N. Martín, *Chem. Rev.* **1999**, *99*, 3199–3246.
[32] M. Winkler, J. O. Mueller, K. K. Oehlenschlaeger, L. Montero de Espinosa, M. A. R. Meier, C. Barner-Kowollik, *Macromolecules* **2012**, *45*, 5012–5019.
[33] K. K. Oehlenschlaeger, J. O. Mueller, N. B. Heine, M. Glassner, N. K. Guimard, G. Delaittre, F. G. Schmidt, C. Barner-Kowollik, *Angew. Chem. Int. Ed.* **2013**, *52*, 762–766.
[34] D. S. Tyson, F. Ilhan, M. A. B. Meador, D. D. Smith, D. A. Scheiman, M. A. Meador, *Macromolecules* **2005**, *38*, 3638–3646.
[35] F. G. Schmidt, S. Hilf, C. Barner-Kowollik, N. Guimard, K. K. Oehlenschlaeger, J. Mueller, *DE102012200235A1*, **2013**
[36] G. G. Odian, Principles of Polymerization. 4th ed., Wiley, Hoboken, NJ **2004**.
[37] B. T. Storey, *J. Polym. Sci. Part A* **1965**, *3*, 265–282.
[38] K. M. Ho, C. T. Chan, C. M. Soukoulis, R. Biswas, M. Sigalas, *Solid State Commun.* **1994**, *89*, 413–416.
[39] M. Hesse, H. Meier, B. Zeeh, Spectroscopic Methods in Organic Chemistry 2nd ed., Thieme, Stuttgart **2007**.
[40] R. N. Keller, H. D. Wrcoff, L. E. Marchi, in Inorganic Syntheses John Wiley & Sons, Inc., Hoboken, NJ **2007**, pp. 1–4.
[41] T. Pauloehrl, G. Delaittre, V. Winkler, A. Welle, M. Bruns, H. G. Börner, A. M. Greiner, M. Bastmeyer, C. Barner-Kowollik, *Angew. Chem. Int. Ed.* **2012**, *51*, 1071–1074.
[42] G. Mantovani, F. Lecolley, L. Tao, D. M. Haddleton, J. Clerx, J. J. L. M. Cornelissen, K. Velonia, *J. Am. Chem. Soc.* **2005**, *127*, 2966–2973.
[43] S. Varaprath, P. J. Varaprath, *US4861906*, **1989.**
[44] J. Fischer, J. B. Mueller, J. Kaschke, T. J. A. Wolf, A.-N. Unterreiner, M. Wegener, *Opt. Express* **2013**, *21*, 26244–6260.